

## Arsenic trisulfide-doped silica-based porous glass

J.A. Burunkova<sup>a</sup>, G. Alkhalil<sup>a</sup>, A.V. Veniaminov<sup>a</sup>, I. Csarnovics<sup>b,\*</sup>, S. Molnar<sup>c</sup>, S. Kokenyesi<sup>b</sup>

<sup>a</sup> ITMO University, Saint Petersburg 197101, Russia

<sup>b</sup> University of Debrecen, Faculty of Science and Technology, Institute of Physics, Debrecen 4032, Hungary

<sup>c</sup> Institute of Nuclear Research, ELKH Institute, Debrecen 4026, Hungary

### ARTICLE INFO

#### Keywords:

Porous silica glass  
Amorphous chalcogenides  
Nanocomposites  
Light- and thermally induced effects

### ABSTRACT

Novel composite material based on silica porous glass as low refractive index matrix and high refractive index  $As_2S_3$  nanoparticles filled in the pores has been made. Chalcogenide nanoparticles were dissolved and the porous glass matrix was impregnated in the obtained solution. Subsequently, the solvent was evaporated by annealing the porous glass. Various optical parameters of the created composite material are presented in this paper. These parameters are based on optical and structural transformations which occur under active illumination and heat treatment in such chalcogenide-containing composite and compared with thin  $As_2S_3$  light-sensitive layers. New functionalities may be added this way to the composite, such as illumination and/or thermally driven optical parameters. Developing and optimizing the optical properties of the obtained  $As_2S_3$ -porous glass composites can be useful for creating 3D optical-structural patterns for different applications such as holographic data storage, light modulation, and/or functional, nonlinear optical elements with various parameters for VIS-NIR optics.

### 1. Introduction

Silicon dioxide ( $SiO_2$ ) is known to be the most ubiquitous material in optical media. This predominant presence of  $SiO_2$  is due to its unique physicochemical properties, optical transparency, as well as mechanical hardness, heat resistance, electrical strength, optical stability, and chemical resistance [1]. One way for further expansion of the silicate glass applications is silicate-based porous glasses.

Porous silicate glass (PG) is a glass with nanometer or micrometer pores and is usually prepared by metastable phase separation in borosilicate glasses, followed by liquid extraction of one of the formed phases [2]. The possibility to be produced with different texture parameters, as well as the unique physical properties of the silicate glass matrix, such as the optical transparency, mechanical hardness, and heat resistance has made PG an ideal material for various applications. The applications of porous glasses can be classified into two main groups. The first one concerns using PG in material processing, such as material separation or membrane reactors [3–5]. For example, in [3], membranes of surface-modified porous glass have shown a highly selective separation of hydrocarbon gases. In [5], porous glass impregnated with Pd was employed as a catalyst for chemoselective hydrogenation reactions. The second group of applications investigates the possibility to obtain PG composites with desired properties by impregnating PG with different

substances (metals, semiconductors, liquid crystals) [6–8]. The confinement effect in PG represents another interesting research topic [7–8].

Composite materials based on chalcogenide glasses (ChGs) represent an important and growing class of materials due to their promising physical and optical characteristics as well as a broad range of applications [9]. Moreover, ChGs possess unique metastability and, as a consequence, they are susceptible to photo structural changes induced by bandgap energy illumination [10]. These structural changes are accompanied by changes in the optical properties, such as the optical absorption edge and refractive index, and they can be reversible, i.e., deleted by thermal treatment or illumination. [11–12]. ChGs in the form of glasses or thin films have been well-studied [12–13]. ChG films are usually obtained either by thermal spraying or by deposition from alkali or amine solvent with dissolved ChGs [14–15]. Investigations of polymer composite materials with ChGs were also performed by introducing them into polymer solutions with the subsequent preparation of films by the spin-coating method [16–17].

In [18], nanocomposites based on a mixture of urethane-acrylates with  $As_2S_3$  or  $As_2Se_3$  were obtained, the photoinduced properties were investigated, and a holographic recording of Bragg grating was carried. In [19],  $As_2S_3$  melt was introduced into the porous glass and the optical characteristics such as the refractive index, Raman spectrum, and the

\* Corresponding author at: 18/a Bem sq, Debrecen 4026, Hungary.  
E-mail address: [csarnovics.istvan@science.unideb.hu](mailto:csarnovics.istvan@science.unideb.hu) (I. Csarnovics).

optical absorption spectrum in the vicinity of the fundamental bandgap were investigated.

Inserting ChG nanoparticles with a high refractive index ( $n \approx 2.8\text{--}3.2$  in VIS-NIR regions) into the PG can increase the average  $n$  of the media, realize high modulation characteristics, as well as produce materials with high transparency and optical nonlinearity in the NIR spectral region. The nanoscale dimensions of particles at comparatively low concentrations in a glass matrix ensure the low scattering in the VIS-IR spectral regions. An additional advantage of such material could be the possibility to change the optical parameters of the inserted semiconductor chalcogenide glass particles (optical band gap, refractive index, and luminescence properties) by special illumination and annealing, which gives the possibility to varying the parameters of the final optical element [20].

In this paper, we present the fabrication route and optical properties of light-sensitive nanocomposites based on PG doped with high-refractive-index chalcogenide nanoparticles (refractive index about 2.2 in the vis-NIR region) with new, useful optical properties. Structural, optical parameters and light-heat-induced changes were studied in this composite and compared to the pure chalcogenide layer. The luminescence of chalcogenide doped PG was also investigated. The luminescence of ChG glasses or deposited thin films was studied before, at low temperatures or elevated pressures and mainly in the IR region [21–24]. However, the transition to the nanoscale can introduce changes in the properties of substances and such studies for ChG are practically absent. Such 3D materials based on porous glasses filled with ChG could hold promise for applications in different spectral ranges, the VIS-NIR, or even the terahertz range [25].

## 2. Experimental details

### 2.1. Materials

For the fabrication of PG, we followed the same procedures as in [26]. Sodium-borosilicate DV-1 glass with the composition 7 % Na<sub>2</sub>O-23% B<sub>2</sub>O<sub>3</sub>-70% SiO<sub>2</sub>, heat-treated at 530 °C for 70–72 h, then at 465 °C for three-four hours was used. The glasses were corroded in an aqueous HCl solution at a constant temperature of 50 °C for about eight days. The glass to solution ratio was 1.6/100 g/ml. After leaching, the samples were washed several times with distilled water and left to air dry at room temperature for two days, and then they were dried at 120 °C for two hours.

Small pieces of PG (7 × 10 mm, 3.6 mm thickness) were used. According to [26], the obtained samples have an average pore size of about 10 nm and a specific surface area ranging from 10 to 300 m<sup>2</sup>/g. Moreover, we examined the pore volume of the prepared porous glass samples. Based on the sorption capacity of both water and ethyl alcohol for the prepared porous glasses, the pore volume was estimated to form about 30% of the total glass volume.

### 2.2. Creation of nanocomposite samples

A simple chemical dissolution method was used for doping PGs with As<sub>2</sub>S<sub>3</sub>. At the first step, small pieces of As<sub>2</sub>S<sub>3</sub> glass were ground and dissolved in propylamine; solutions with different concentrations of As<sub>2</sub>S<sub>3</sub> (3.1, 6.0, and 11.0 mg/ml) were prepared. It is known that the chains-layered structure of As<sub>2</sub>S<sub>3</sub>, breaks in amines solutions into amorphous fragments with a dimension less than 1 nm [27]. The next step was PG impregnation in these solutions for three-seven days, i.e. for different volume concentrations of particles in PG. The solutions were placed in the nitrogen atmosphere to avoid possible As<sub>2</sub>S<sub>3</sub> oxidation. After the impregnation, the samples were extracted from the solution and left to air dry for one hour, and then they were dried at 120 °C for two-four hours. The obtained glass samples were light yellow colored, homogeneous and transparent, and after annealing for four hours at 120–140 °C, the sample's color turned to light yellow, orange or brown

depending on the As<sub>2</sub>S<sub>3</sub> concentration (Fig. 1). Such color-changing of As<sub>2</sub>S<sub>3</sub> thin films upon irradiation and annealing is well-known [28]. The sample mass was measured before and after impregnation to define the As<sub>2</sub>S<sub>3</sub> concentration in PGs.

As<sub>2</sub>S<sub>3</sub> concentration in PGs was calculated from the difference in the sample's mass before and after impregnation and was considered to be the ratio of As<sub>2</sub>S<sub>3</sub> mass in PG to the mass of the pure PG (before impregnation). As result, four kinds of samples with different concentrations were obtained: 1 wt%, 2 wt%, 3.6 wt%, and 3.9 wt%. A sample with 3.9 wt% As<sub>2</sub>S<sub>3</sub> concentration was dark brown colored with high absorption, therefore could not be studied using the transmission spectrum in the visible range. Samples with 1 wt%, 2 wt% were bright yellow-colored and exhibited a slight shift in the transmission spectrum under the illumination. On the other hand, samples with a 3.6 wt% concentration were transparent, orange-colored, and exhibited a large shift in the transmission spectrum under additional treatments; therefore, they were selected for further measurements and investigations in this research.

The created PG nanocomposites were compared with the thin As<sub>2</sub>S<sub>3</sub> layer (As<sub>2</sub>S<sub>3</sub>-TF) and polymer nanocomposites doped with As<sub>2</sub>S<sub>3</sub> (As<sub>2</sub>S<sub>3</sub>-P). For the thin layer samples, bulk chalcogenide glasses from the As-S system were synthesized in silica ampoules from high-purity (typically 99.999 %) elements by the melt-quenching method and used for the deposition of amorphous layers via thermal evaporation at  $1 \times 10^{-6}$  mbar pressure; their thickness was 2 μm. The creation technology of the nanocomposite samples based on As<sub>2</sub>S<sub>3</sub>-P was described in [29].

### 2.3. Investigation of the created nanocomposites

Optical transmission spectra of the samples were measured in the visible-near infrared spectral region by the standard method using the Fluorat-02-Panorama spectrofluorometer. As<sub>2</sub>S<sub>3</sub>-doped PG samples were investigated under illumination with green laser 532 nm KLM-532/h/1000, and the annealing of the nanocomposite samples was done at 150 °C at atmospheric pressure.

The composition of the created samples was determined by Energy Dispersive X-Ray Spectroscopy (EDS) using a Hitachi S-4300 Scanning Electron Microscope (SEM) system. The SEM was used for the investigation of the structure of the nanocomposites, while the structure and composition were also studied with a Horiba LabRam Raman spectrometer. During the work, a 785 nm laser was used as an excitation source, and the measurement time for each sample was 10 s (to avoid any light-stimulated effects). The excitation beam was focused on the sample surface with a 50× lens. Raman measurements were performed at several points on the substrate surface (five-seven points).

The LSM 710 confocal laser scanning microscope (Carl Zeiss) that operates in the visible range was used to obtain optical and luminescent images of the samples, and to analyze its luminescence properties under the excitation at different wavelengths.

## 3. Results and discussion

We expect that the dissolved As<sub>2</sub>S<sub>3</sub> deposited in PGs is in a form of nanolayers on the walls of the capillaries. Actually, in a similar experiment, a solution-based material was reported to form nanometer layers of amorphous films inside the cylindrical air channels of silica-based photonic crystal fiber (PCF) [30]. In the reported work, the existence of nanolayers was directly confirmed by cross-section SEM images of cleaved pieces of PGs. We suppose, that, if thin films on the walls are formed, their thickness can be estimated as follows.

The average As<sub>2</sub>S<sub>3</sub> layer thickness in PG:

$$d = \frac{m}{S \cdot \hat{A} \cdot p} = \frac{0.015}{3.43 \hat{A} \cdot 10^4 \cdot 0.411 \hat{A} \cdot 10^4} = 1.06 nm,$$

where  $m = 0.015$  g is As<sub>2</sub>S<sub>3</sub> As<sub>2</sub>S<sub>3</sub> mass in PG;  $p = 3.43$  g/cm<sup>3</sup> is

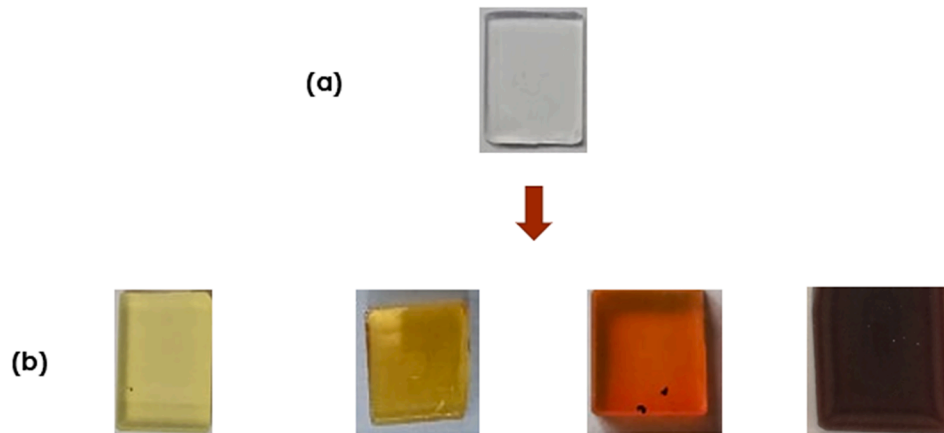


**Fig. 1.** Image of PG sample ( $\sim 12 \times 18$  mm) before (a) and after (b) impregnation in  $\text{As}_2\text{S}_3$  solution ( $\text{As}_2\text{S}_3$  the concentration from left to right 1 wt%, 2 wt%, 3.6 wt%, 3.9 wt%).

$\text{As}_2\text{S}_3$  density;  $S = 10 \times 0.411 \times 10^4 \text{ cm}^2$  is the specific surface area of pores in PG ranging from 10 to  $300 \text{ m}^2/\text{g}$  (here the minimum value was considered). However, the formation of the nano-grained layer of  $\text{As}_2\text{S}_3$  nanoparticles in the pores is also possible. In both cases, the nano dimension influence on optical properties is seen, since a blue-shift of optical absorption edge is observed in comparison with thick  $\text{As}_2\text{S}_3$  layers.

### 3.1. SEM results

Scanning EM was used to confirm the presence of  $\text{As}_2\text{S}_3$  inside the PG pores. Fig. 2 demonstrates a cleaved piece from the PG sample doped with  $\text{As}_2\text{S}_3$ . The dark spots correspond to pores at the surface. This image was analyzed to estimate the average pore size which was found to be about 23 nm. Moreover, a compositional analysis of the sample was conducted to examine the presence of As and S atoms in PG. The presence of As in PG is well-defined (see Fig. 3), but the presence of S can not be confirmed, due to the large overlap between its corresponding peaks and O peaks, as well as the destroying effects of higher excitation intensities, necessary to select S element in EDS spectra.

### 3.2. Optical parameters

The optical transmission spectra of pure PG and  $\text{As}_2\text{S}_3$ -PG samples under one cycle of illumination and annealing were measured and compared with the transmission spectra of the  $\text{As}_2\text{S}_3$  thin layer (Fig. 4). As we can see from Fig. 4, the transmission spectrum shifts to shorter wavelengths (from curve 2 to 3) under the illumination for 150 min with

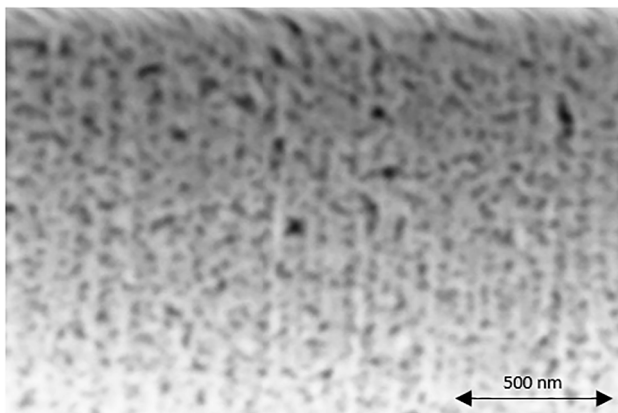


**Fig. 2.** SEM image of  $\text{As}_2\text{S}_3$  impregnated PG cleaved surface.

the power intensity of  $200 \text{ mW}/\text{cm}^2$ , and it returns almost to its initial location after annealing for 90 min at  $150 \text{ }^\circ\text{C}$  (from curve 3 to 4). The transmission spectra of the  $\text{As}_2\text{S}_3$  thin layer were measured in their initial state, after 100 min-illumination with the power density of  $85 \text{ mW}/\text{cm}^2$  and then after additional annealing for 90 min at  $200 \text{ }^\circ\text{C}$ . The transmission spectrum shifts to longer wavelengths (from curves 5 to 6, Fig. 4), and it returns almost to its initial position after annealing (from curves 6 to 7, Fig. 4).

The transmission spectra were used for the calculation of the absorption coefficient  $\alpha$  (Fig. 5). The linear section of the absorption was employed for the calculation of the bandgap energy and the clear exponential drop for the calculation of Urbach energy for  $\text{As}_2\text{S}_3$  in this composite before and after illumination (Fig. 5).

The bandgap energy of the nanocomposite in the as-deposited state was found to be 2.43 eV, which is blue-shifted by 0.12 eV compared to the bandgap energy of 2.35 eV of vacuum evaporation deposited  $\text{As}_2\text{S}_3$  thin films. The  $\text{As}_2\text{S}_3$ -PG composite, after illumination, exhibits a 0.23 eV shift in the bandgap energy to 2.66 eV, and after annealing for 90 min at  $150 \text{ }^\circ\text{C}$  the bandgap shifts back to  $E_g = 2.47 \text{ eV}$ ; however, it does not reach the initial state. Urbach energy, after illumination, decreases from  $E_u = 0.313 \text{ eV}$  to  $E_u = 0.304 \text{ eV}$ . Urbach energy is known to account for the structural disorder, defects in materials and it decreases with Eg increasing after ordering. Thus, the photo-induced changes accompanied by the decrease in Urbach energy can be attributed to the decrease of the amorphous state and the related density of localized band gap states within the  $\text{As}_2\text{S}_3$  phase in PG. Such rather large bandgap changes towards structural ordering may be connected with oriented interactions between chalcogenide clusters and active pore surfaces.

A reversible photo-bleaching effect (PB) was observed in  $\text{As}_2\text{S}_3$ -PG composite after illumination and photo-darkening (PD) after annealing (Fig. 4). This reversible PB is opposite to the typical PD effect (the redshift of the optical absorption edge) observed in chalcogenide glasses. Reversible PB was observed before in chalcogenides thin films with a thickness less than 90 nm [31] and is considered to be a nanosized effect due to the increase of the surface/volume ratio. In our samples, since the size of the deposited material is restricted by the size of the pores which is in the nanometer range, this can explain the observed reversible PB effect as a nanosized effect [31]. However, our experiments were performed at room temperature, different from [31], where reversible PB can be observed only above a given temperature, called the optical bleaching threshold. Moreover, we also observed a similar reversible PB effect in  $\text{As}_2\text{S}_3$ -polymer nanocomposites ( $\text{As}_2\text{S}_3$ -P) [29]. The  $\text{As}_2\text{S}_3$ -P nanocomposite undergoes reversible PB upon illumination, and the bandgap increases from 2.2 to 2.25 eV. The PB can be reversed by heat treatment and the bandgap decreases from 2.25 to 2.08 eV (the further decrease in the bandgap energy could be explained by the

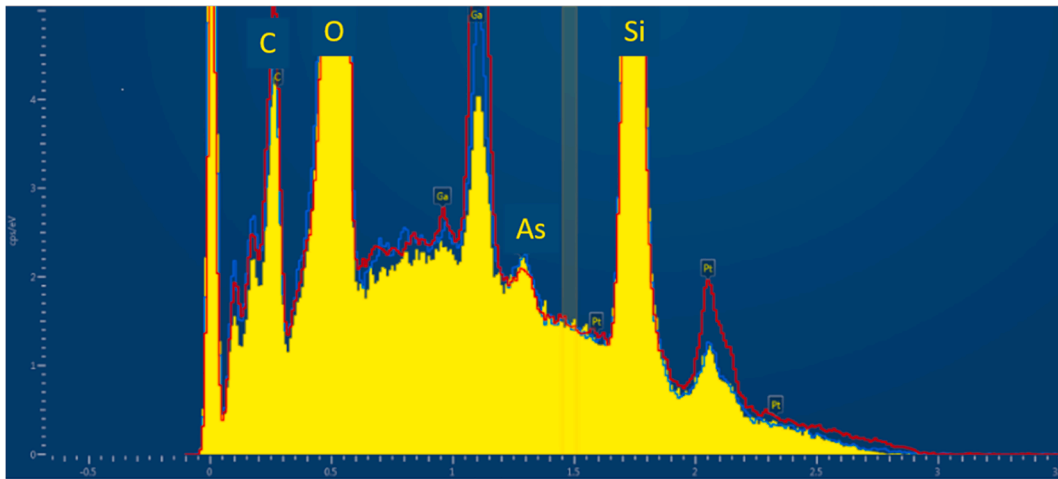


Fig. 3. Composition of As<sub>2</sub>S<sub>3</sub>-PGs using EDX.

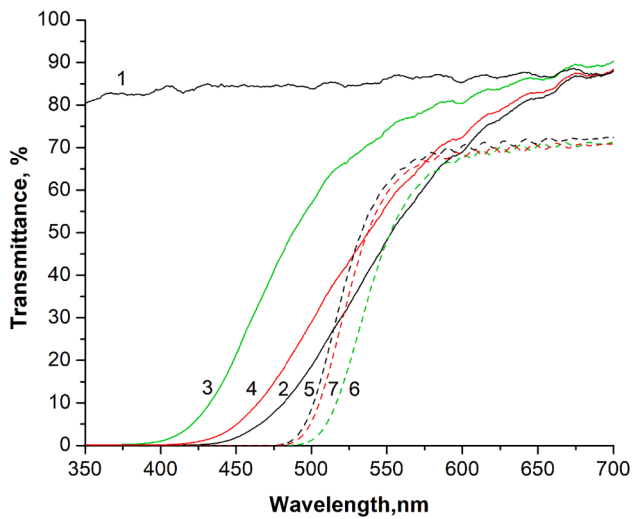


Fig. 4. Optical transmission spectra: pure porous glass (1), an initial sample of As<sub>2</sub>S<sub>3</sub>-PG composite (2), an illuminated sample of As<sub>2</sub>S<sub>3</sub>-PG composite (3), an illuminated-annealed sample of As<sub>2</sub>S<sub>3</sub>-PG composite (4), an initial sample of As<sub>2</sub>S<sub>3</sub> thin layer (5), an illuminated sample of As<sub>2</sub>S<sub>3</sub> thin layer (6), an illuminated-annealed sample of As<sub>2</sub>S<sub>3</sub> thin layer (7).

polymer expansion under annealing) [29].

The results for the As<sub>2</sub>S<sub>3</sub>-PG composite are presented and compared with As<sub>2</sub>S<sub>3</sub>-TF and As<sub>2</sub>S<sub>3</sub>-P nanocomposite (from [29] in Table 1. (The data for As<sub>2</sub>S<sub>3</sub>-TF and As<sub>2</sub>S<sub>3</sub>-P was taken from [29].)

The following points summarize the differences found by comparing As<sub>2</sub>S<sub>3</sub>-PG nanocomposite, As<sub>2</sub>S<sub>3</sub>-TF, and As<sub>2</sub>S<sub>3</sub>-P nanocomposite:

- 1- There are differences in the structure of evaporated As<sub>2</sub>S<sub>3</sub> layer, and As<sub>2</sub>S<sub>3</sub> in PG. When it comes to the photoinduced effects, the As<sub>2</sub>S<sub>3</sub> deposited films behave like bulk materials, while As<sub>2</sub>S<sub>3</sub> in PG and polymer matrices have a nanoscale structure with possibly different bonding defects and the confinement effect.
- 2- Both prepared As<sub>2</sub>S<sub>3</sub>-PG and As<sub>2</sub>S<sub>3</sub>-P composites exhibit the photo-bleaching effect, which is the opposite behavior of As<sub>2</sub>S<sub>3</sub> in thin films deposited by not intensive, comparatively slow thermal evaporation in a vacuum (photodarkening).
- 3- The initial state of As<sub>2</sub>S<sub>3</sub>-PG can not be restored after annealing, which means, there are reversible and irreversible changes involved in the photoinduced transformations of as-deposited films in pores.

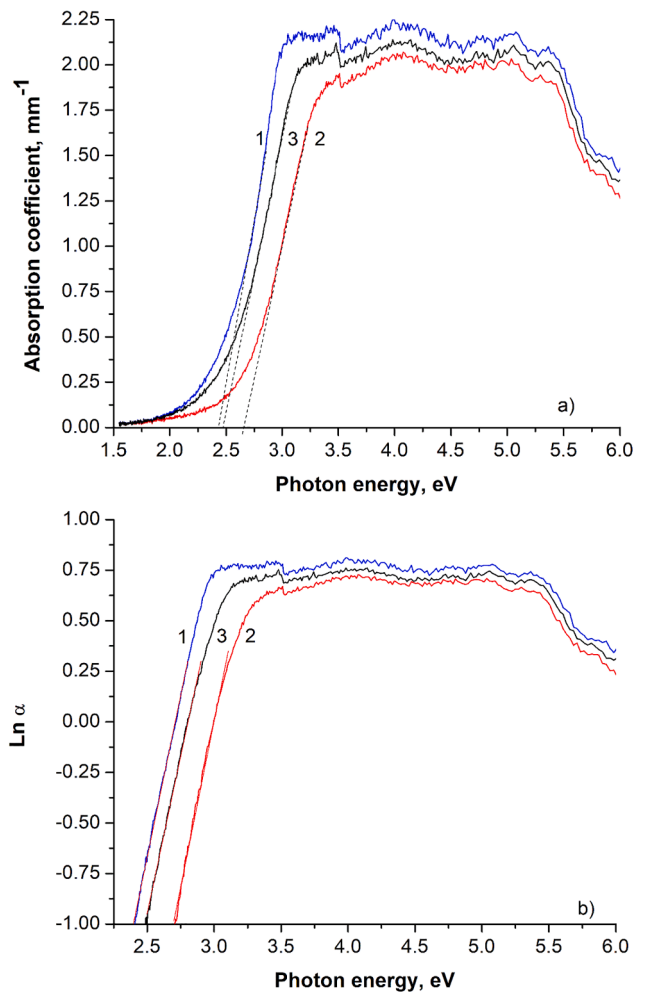


Fig. 5. (a) The absorption coefficients versus photon energy, (1) the initial spectrum  $E_g = 2.43$  eV, (2) after illumination for 150 min with a power intensity of 200 mW/cm<sup>2</sup>  $E_g = 2.66$  eV  $E_g = 2.66$  eV, (3) after annealing for 90 min at 150 °C  $E_g = 2.47$  eV (b) Urbach plot for As<sub>2</sub>S<sub>3</sub>-PG composite before illumination (1), after illumination (2), and after annealing (3).

- 4- The shift in bandgap energy in As<sub>2</sub>S<sub>3</sub>-PG (0.23 eV) is higher than the shift in both As<sub>2</sub>S<sub>3</sub>-TF (0.07 eV) and As<sub>2</sub>S<sub>3</sub>-P composite (0.03 eV). This can be ascribed to the high free volume of As<sub>2</sub>S<sub>3</sub> nanolayers in

**Table 1**

Comparison of the annealing and illumination influence on the bandgap energy of  $\text{As}_2\text{S}_3$  for different composite.

	$\text{As}_2\text{S}_3$ -PG		$\text{As}_2\text{S}_3$ -TF		$\text{As}_2\text{S}_3$ -P	
	$E_g$ (eV)	$E_u$ (eV)	$E_g$ (eV)	$E_u$ (eV)	$E_g$ (eV)	$E_u$ (eV)
Initial	2.43	0.313	2.35	0.111	2.22	0.33
After illumination 532 nm	2.66	0.304	2.27	0.113	2.25	0.33
After heat treatment	2.47	0.322	2.33	0.120	2.08	0.33

PG, which gives more flexibility for photo-structural transformation. Whereas, in the deposited films, to some extent, the stacked-layer structure hinders the photo-structural transformation.

- 5- The photoinduced changes in  $\text{As}_2\text{S}_3$ -PG accompanied by the decrease of Urbach energy are attributed to the decrease of the amorphous state and the related density of localized states within the  $\text{As}_2\text{S}_3$  phase in PG. The orientational influence of active surfaces in pores may stimulate this process.

### 3.3. Investigation of the nanocomposite structure

The Raman spectra of pure PG,  $\text{As}_2\text{S}_3$ -PG composite,  $\text{As}_2\text{S}_3$ -TF, and  $\text{As}_2\text{S}_3$ -P composite were measured (Fig. 6).

To start with, the Raman spectrum of  $\text{As}_2\text{S}_3$ -TF includes the conventional bands that correspond to the arsenic sulfide glasses in general. The most intense and broadband around  $360\text{ cm}^{-1}$  is assigned to As-S bond stretching vibrations of  $\text{As}_2\text{S}_3$  and  $\text{As}_4\text{S}_4$  tetrahedral and contains several Raman lines [32]. The bands  $150\text{--}190\text{ cm}^{-1}$  and  $485\text{ cm}^{-1}$  are assigned to the vibrations of S atoms in the  $\text{S}_8$  rings [33]. The bands  $235\text{--}273\text{ cm}^{-1}$  correspond to the vibrations of homopolar As-As bonds in the realgar  $\text{As}_4\text{S}_4$  units [32–33]. All these bands were also observed in the spectrum of the  $\text{As}_2\text{S}_3$ -polymer composite, where the similarity between the two spectra is clear, mainly due to the rather large, about  $20\text{--}30\text{ nm}$  chalcogenide nanoparticles, which may be clusters of smaller particles [18].  $522\text{ cm}^{-1}$  – the weak band corresponds to the vibration of the  $\text{As}_4\text{S}_4$  or  $\text{As}_4\text{S}_6$  structures. These structures can form in an amorphous glass of arsenic sulfide [34].

The  $168$ ,  $235$ ,  $273$ , and  $330\text{ cm}^{-1}$  bands assigned to As-As bond stretching vibrations and As-S bond stretching vibrations, respectively; and the  $190\text{ cm}^{-1}$  and  $485\text{ cm}^{-1}$  assigned to the vibrations of S atoms in the  $\text{S}_8$  rings were observed in the Raman spectrum of  $\text{As}_2\text{S}_3$ -PG. The  $110$ ,  $115$ ,  $485$ ,  $522$ , and  $640\text{ cm}^{-1}$  bands represent the contribution of the

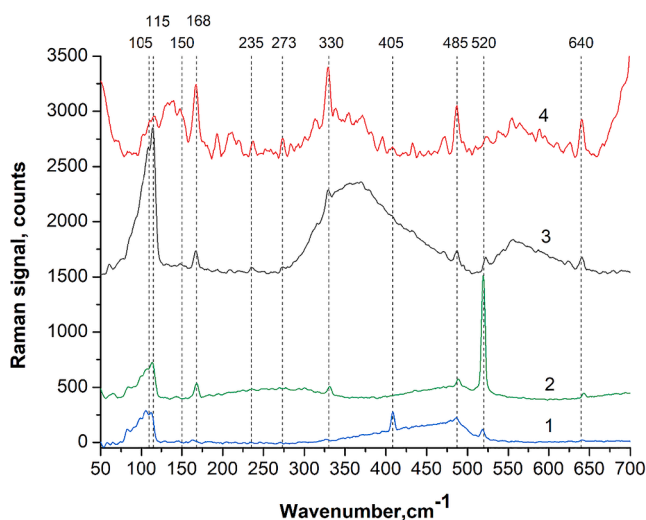


**Fig. 6.** Raman spectrum of pure PG (1),  $\text{As}_2\text{S}_3$ - $\text{As}_2\text{S}_3$ -PG (2),  $\text{As}_2\text{S}_3$ -TF (3),  $\text{As}_2\text{S}_3$ - $\text{As}_2\text{S}_3$ -P composite (4).

silicate glass substrate to the Raman spectrum, and some of these bands were observed in PG spectra as well [35–36].

Some differences in Raman spectra appeared in  $\text{As}_2\text{S}_3$ - $\text{As}_2\text{S}_3$ -PG samples: the  $408\text{ cm}^{-1}$  bands from pure PG disappeared and the narrow band at  $520\text{ cm}^{-1}$  increases strongly. Following the above-mentioned model, this may be explained by the orientational influence of active pore surfaces, due to interconnections between Si-O groups of pore surface and As-S ones in chalcogenide NP. It is also possible, that among the photo-induced changes an oxidation process [37] occurs during illumination-heat treatment, and plays some role in changing the composite structure, optical properties, but the preservation of typical yellow–red colors (see Fig. 1) i.e. band gaps of  $\text{As}_2\text{S}_3$  does not refer to it. Due to the above-mentioned interactions the wideband at  $360\text{ cm}^{-1}$ , which is assigned to As-S bond stretching vibrations, decreases in parallel with its shift towards lower,  $250\text{--}300\text{ cm}^{-1}$  frequency range due to the possible influence of size- and deformation effects in nano dimensional elements [38].

### 3.4. Creation of structures on the nanocomposites

We tried to employ these huge photo-induced changes of  $\text{As}_2\text{S}_3$ -PG composite for the holographic recording of diffraction gratings, but there was found no trace for any grating. We suppose that the multiple scattering in the porous structure results in homogenous illumination of the whole sample, and this can be the reason why no specific pattern of illumination was recorded. Therefore, to avoid the internal reflection in pores, one solution was to fill the pores with some polymeric filler with a refractive index close to the PG refractive index.

The fabrication method of the sample for optical recording is as follows: porous glass sample was impregnated for two weeks in a monomeric solution of the composition (diurethane dimethacrylate (UDMA) 20 wt%, 2-phenoxyethyl acrylate (PEA) 10 wt%, 2-carboxylate 20 wt%, butyl acrylate 50 wt%) with  $\text{As}_2\text{S}_3$  (7.5 wt% of monomer mixture) and with Irgacure 784 as an initiator (5 wt% of monomer mixture). The monomers were selected in a way that they modify the surface of the nanoparticles to blend without aggregation [29].

After impregnation, the sample was light yellow colored and transparent. It was irradiated with  $532\text{ nm}$  with a power density of  $25\text{ mW/cm}^2$  for  $75\text{ min}$  to initiate the polymerization process; the sample color turned cloudy light yellow. After that, it was heat-treated at  $T = 120\text{--}130\text{ }^\circ\text{C}$  for  $24\text{ h}$ , and its color became dark brown. The grating was successfully recorded on the obtained sample with a TEM grid mask (Fig. 7), using  $532\text{ nm}$  laser light with  $200\text{ mW/cm}^2$  power density, and it was studied by a confocal microscope.

The influence of photoinduced changes on electron processes in such material was investigated by measuring the photoluminescence spectra (PL) of the irradiated and un-irradiated regions under the excitation with two different photon energies  $E_{\text{ex}} = 2.28\text{ eV}$  and  $E_{\text{ex}} = 3.06\text{ eV}$  (Fig. 8). Also, for comparison, the PL spectrum of  $\text{As}_2\text{S}_3$ -PG filled with butyl acrylate and the PL of Irgacure 784 was measured with the excitation energy of  $3.06\text{ eV}$ .

Comparing the PL spectra of  $\text{As}_2\text{S}_3$ -PG polymer composite and Irgacure 784, we can notice that the characteristics of the Irgacure 784 PL spectrum are presented in the PL spectrum of  $\text{As}_2\text{S}_3$ -PG polymer; however, the main intensive bands of the latter are not assigned to Irgacure 784. This observation as well as the similarity in the spectra of  $\text{As}_2\text{S}_3$ -PG polymer and  $\text{As}_2\text{S}_3$ -PG filled with butyl acrylate prove that the origin of photoinduced changes in the PL spectrum of  $\text{As}_2\text{S}_3$ -PG polymer composite is  $\text{As}_2\text{S}_3$  but not Irgacure 784 (see Fig. 8).

The main intensive band in the PL spectra of  $\text{As}_2\text{S}_3$ -PG polymer composite was observed at  $2.54\text{ eV}$  when excitation photon energy was  $3.06\text{ eV}$ . The peak intensity of this band was higher for the irradiated regions than the peak intensity of the un-irradiated regions. The opposite effect was observed when the excitation photon energy decreased to  $2.28\text{ eV}$ , the main intensive band found at  $2.08\text{ eV}$  and it was higher for the un-irradiated regions. This observation can be explained by the

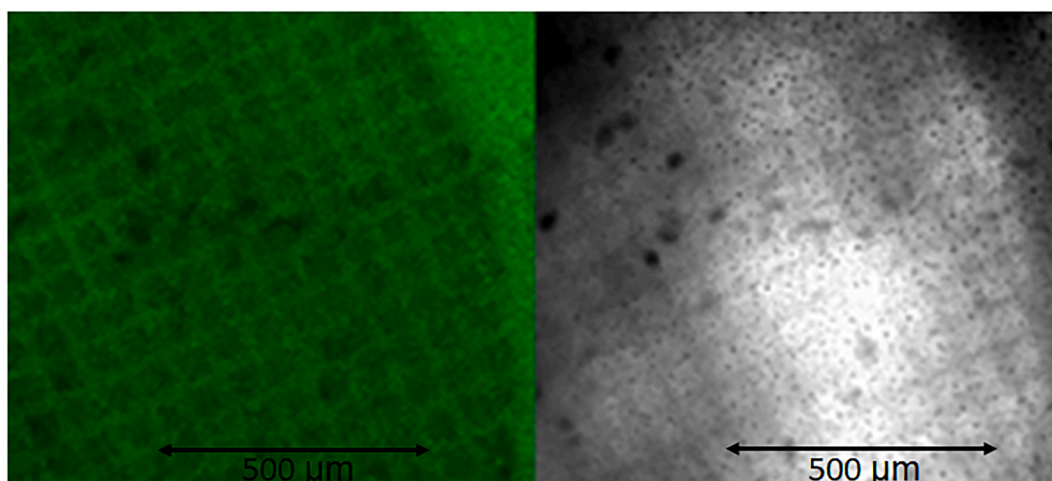


Fig. 7. Confocal microscope image of the grid recorded through a TEM grating mask in the reflected (left, irradiated with a 543 nm laser) and transmitted (right, white light) mode.

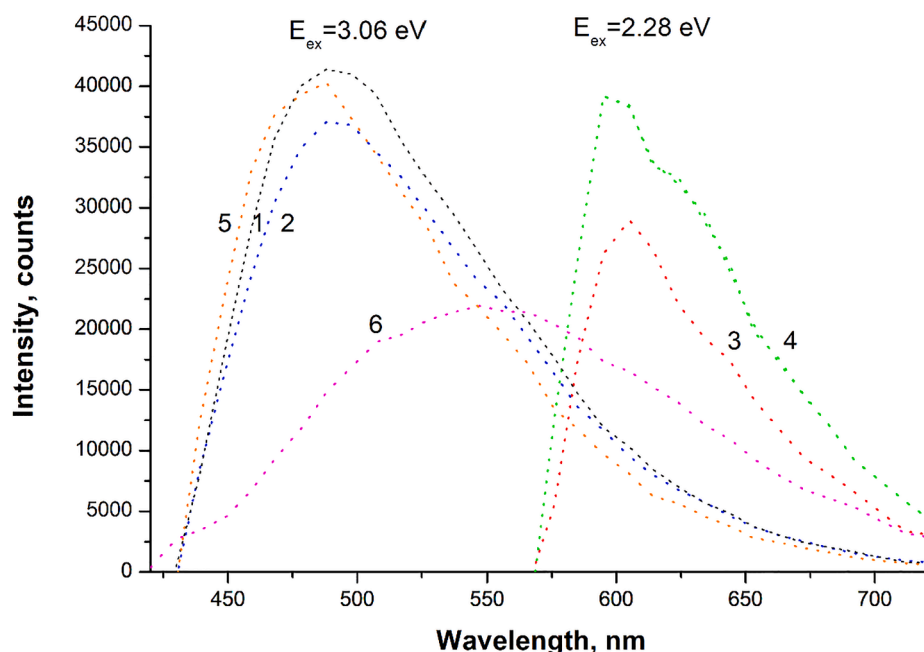


Fig. 8. Photoluminescence spectra of  $\text{As}_2\text{S}_3$ -PG polymer composite with two different excitation energies: 3.06 and 2.28 eV (1 and 3 - irradiated region, 2 and 4 - unirradiated region),  $\text{As}_2\text{S}_3$ -PG filled with butyl acrylate (5), and Irgacure 784 (6).

creation of optically-induced states in the illuminated regions, with excitation energies higher than 2.28 eV.

#### 4. Conclusion

In this paper, we have presented the fabrication route of new composite material based on porous glass and  $\text{As}_2\text{S}_3$  nanolayers formed on the walls of the pores. Several light-induced changes in the optical properties, such as the change in transmission spectra, optical band gap, and luminescence have been observed and discussed. This composite exhibits a giant reversible photo-induced bleaching effect up to 50% of optical transmission in the selected spectral range accompanied by an increase in the bandgap energy by 0.23 eV. The prepared  $\text{As}_2\text{S}_3$ -porous glass and  $\text{As}_2\text{S}_3$ -polymer composites exhibit the photo-induced effect, which is the opposite behavior of  $\text{As}_2\text{S}_3$  in thin films deposited by thermal evaporation in a vacuum (photo-darkening). The initial state of the  $\text{As}_2\text{S}_3$ -porous glass composite can not be restored after first

annealing, which indicates that there are reversible and irreversible changes involved in the photoinduced transformations of films in pores. These changes can be attributed partially to the known effects of reversible-irreversible structural and optical effects in  $\text{As}_2\text{S}_3$  and partially to the confinement effect by the nanosized pores of the porous glass. The last may be connected with orientational actions of pore walls, resulting in connections between Si-OH groups of silicate and As-S groups of chalcogenide.

Structural investigations and compositional analyses have been performed using SEM spectroscopy and Raman scattering measurements to confirm the presence of  $\text{As}_2\text{S}_3$  inside the porous glass. The photo-induced changes have been successfully employed for model grid pattern recording using green laser light, and the obtained grid pattern has been investigated by confocal microscopy. The developed material possesses additional functionality: photoluminescence in the visible spectral range.

Developing and optimizing the optical properties of the  $\text{As}_2\text{S}_3$ -porous

glass composites can be useful for creating 3D optical-structural patterns with variable optical parameters, high refractive index, and luminescence for different applications such as holographic data storage or functional optical elements for visible-infrared optics.

### Declaration of Competing Interest

The authors declare that they have no known competing financial interests or personal relationships that could have appeared to influence the work reported in this paper.

### Acknowledgment

This work was financially supported by the grant GINOP-2.3.2-15-2016-00041. The project is co-financed by the European Union and the European Regional Development Fund. Istvan Csarnovics is grateful for the support of the János Bolyai Research Scholarship of the Hungarian Academy of Sciences (BO/348/20) and the support through the New National Excellence Program of the Ministry of Human Capacities (ÚNKP-21-5-DE-464).

The authors would also like to express their gratitude to Illes L. for the technical support.

### References

- [1] M.W. Haynes, ed. CRC Handbook of Chemistry and Physics (92nd ed.). Boca Raton, FL: CRC Press. ISBN 1439855110 (2011).
- [2] C. Shen, Y.J. Wang, J.H. Xu, Y.C. Lu, G.S. Luo, Porous glass beads as a new adsorbent to remove sulfur-containing compounds, *Green Chem.* 14 (4) (2012) 1009, <https://doi.org/10.1039/c2gc16559g>.
- [3] K. Kuraoka, Y. Chujo, T. Yazawa, Hydrocarbon separation via porous glass membranes surface-modified using organosilane compounds, *J. Memb. Sci.* 182 (2001) 139–149.
- [4] R. Schnabel, P. Langer, Controlled-pore glass as a stationary phase in chromatography, *J. Chromatography A* 544 (1991) 137–146.
- [5] C. Schmöger, T. Gallert, A. Stolle, B. Ondruschka, W. Bonrath, Microwave-Assisted Chemoselective Hydrogenation Reactions Incorporating Hydrogen as Reducing Agent, *Chem. Eng. Technol.* 34 (2011) 445–451.
- [6] D. Chen, H. Miyoshi, T. Akai, T. Yazawa, Colorless transparent fluorescence material: Sintered porous glass containing rare-earth and transition-metal ions, *Appl. Phys. Lett.* 86 (2005) 1–3.
- [7] E. Rysiakiewicz-Pasek, R. Poprawski, J. Polanska, A. Sieradzki, Properties of porous glasses with embedded ferroelectric materials, *J. Non-Cryst. Solids.* 352 (2006) 4309–4314.
- [8] J. Werner, K. Otto, D. Enke, G. Pelzl, F. Janowski, H. Kresse, Dielectric investigations of the N-SmB transition in a porous glass, *Liquid Crystals* 27 (10) (2000) 1295–1300.
- [9] R. Tintu, K. Saura, K. Sulakshna, V.P.N. Nampoori, P. Radhakrishnan, S.H. Thomas, Ge<sub>28</sub>Se<sub>60</sub>Sb<sub>12</sub>/PVA composite films for photonic applications, *J. of Non-Oxide Glasses* 2 (2010) 167.
- [10] K. Tanaka, K. Shimakawa, *Amorphous Chalcogenide Semiconductors and Related Materials*, Springer, New York, (2011).
- [11] J. L. Adam, X. Zhang, (Eds.). *Chalcogenide glasses: preparation, properties and applications*. Woodhead publishing (2014).
- [12] M. Popescu, Disordered chalcogenide optoelectronic materials: phenomena and applications, *J. Optoelectron. Adv. Mater.* 7 (4) (2005) 2189–2210.
- [13] K. Shimakawa, Photon effects in chalcogenide glasses, *J. Optoelectron. Adv. Mater.* 9 (10) (2007) 2973–2978.
- [14] R. Tintu, K. Saurav, K. Sulakshna, V.P.N. Nampoori, P. Radhakrishnan, S. Thomas, Ge 28 Se 60 Sb 12 /PVA composite films for photonic applications, *J. Non-Oxide Glasses* 2 (4) (2010) 167–174.
- [15] Y. Zou, L. Moreel, H. Lin, J. Zhou, L. Li, S. Danto, J.D. Musgraves, E. Koontz, K. Richardson, K.D. Dobson, R. Birkmire, J. Hu, *Solution Processing and Resist-Free Nanoimprint Fabrication of Thin Film Chalcogenide Glass Devices: Inorganic-Organic Hybrid Photonic Integration*, Wiley Adv. Optical Mater. 2 (8) (2014) 759–764.
- [16] S. Song, N. Carlie, J. Boudies, L. Petit, K. Richardson, C.B. Arnold, Spin-coating of Ge<sub>23</sub>Sb<sub>7</sub>S<sub>70</sub> chalcogenide glass thin films, *J. Non-Cryst. Solids.* 355 (45–47) (2009) 2272–2278.
- [17] M.S. Iovu, A.M. Andries, S.A. Buzurniuc, V.I. Verlan, E.P. Colomeico, S.V. Robu, New As<sub>2</sub>S<sub>3</sub>: Pr 3<sup>+</sup>-polymer composite materials, *J. Optoelectron. Adv. Mater.* (2006) 8.1257–260.
- [18] J. Burunkova, S. Molnar, V. Sitnikova, D. Shaimadiyev, G. Alkhalil, R. Bohdan, J. Bako, F. Kolotaev, A. Bonyar, S. Kokenyesi, Polymer–chalcogenide glass nanocomposites for amplitude–phase modulated optical relief recording, *J. Mater. Sci.: Mater. Electron.* 30 (10) (2019) 9742–9750.
- [19] V.A. Karavanskii, Y.N. Petrov, Preparation of As<sub>2</sub>S<sub>3</sub>-Porous Glass Composite and Study of Its Optical Properties, *Laser Phys.* 2 (4) (1992) 514–516.
- [20] M.G. Schnoes, L. Dhar, M.L. Schilling, S.S. Patel, P. Wiltzius, Photopolymer-filled nanoporous glass as a dimensionally stable holographic recording medium, *Opt. Lett.* 24 (1999) 658.
- [21] J. Zhang, P. Zhang, B. Ma, S. Dai, W. Zhang, Q. Nie, Enhancing extraction efficiency of mid-infrared fluorescence in chalcogenide glass via photonic crystal, *Opt. Commun.* 364 (2016) 18–23.
- [22] V.M. Mitsa, R.M. Holomb, G. Lovas, M. Ivanda, G.Y. Rudyko, E.G. Gule, I.V. Fekeshgazi, Room temperature visible luminescence in wide band gap chalcogenide glasses, in: (n.d.) 2012 Proceedings of the 35th International Convention MIPRO. IEEE, (2012).
- [23] B.A. Weinstein, Anomalous pressure response of luminescence in c-As<sub>2</sub>S<sub>3</sub> and a-As<sub>2</sub>Se<sub>2</sub> consequences for defect structure in chalcogenides, *Philos. Mag. B Phys. Condens. Matter; Stat. Mech. Electron. Opt. Magn. Prop.* 50 (6) (1984) 709–729.
- [24] A.V. Stronski, O.P. Paiuk, V.V. Strelchuk, I.M. Nasielka, M. Vlček, Photoluminescence of As<sub>2</sub>S<sub>3</sub> doped with Cr and Yb, *Semiconductor Physics Quantum Electron. Optoelectron.* 17 (4) (2014) 341–345.
- [25] M. Zalkovskij, C. Zoffmann Bisgaard, A. Novitsky, R. Malureanu, D. Savastru, A. Popescu, P. Uhd Jepsen, A.V. Lavrinenko, Ultrabroadband terahertz spectroscopy of chalcogenide glasses, *Appl. Phys. Lett.* 100 (3) (2012) 031901, <https://doi.org/10.1063/1.3676443>.
- [26] V.N. Pak, Yu. Yu. Gavronskaya, T.M. Burkat, Porous glasses and nanostructured materials based on them, *Int. J. Experimental Education*, 2, 227 (2015). (in Russian - <https://www.expeducation.ru/ru/article/view?id=6540>).
- [27] T. Kohoutek, T. Wagner, M. Frumar, A. Chrissanthopoulos, O. Kostadinova, S. N. Yannopoulos, Effect of cluster size of chalcogenide glass nanocolloidal solutions on the surface morphology of spin-coated amorphous films, *J. Appl. Phys.* 103 (2008).
- [28] E. Färm, M.J. Heikkilä, M. Vehkamäki, K. Mizohata, M. Ritala, M. Leskelä, M. Kemell, As<sub>2</sub>S<sub>3</sub> thin films deposited by atomic layer deposition, *J. Vac. Sci. Technol. A* 35 (1) (2017) 01B114, <https://doi.org/10.1116/1.4968202>.
- [29] J. Burunkova, S. Molnar, V. Sitnikova, D. Shaimadiyeva, G. Alkhalil, R. Bohdan, J. Bako, F. Kolotaev, A. Bonyar, S. Kokenyesi, Polymer–chalcogenide glass nanocomposites for amplitude–phase modulated optical relief recording, *J. Mater. Sci.: Mater. Electron.* 30 (10) (2019) 9742–9750.
- [30] C. Markos, S.N. Yannopoulos, K. Vlachos, Chalcogenide glass layers in silica photonic crystal fibers, *Optics express* 20 (14) (2012) 14814, <https://doi.org/10.1364/OE.20.014814>.
- [31] P. Knotek, L. Tichy, D. Arsova, Z.G. Ivanova, H. Ticha, Irreversible photobleaching, photorefractive and photoexpansion in Ge<sub>2</sub>S<sub>3</sub> amorphous film, *Mater. Chem. Phys.* 119 (1–2) (2010) 315–318.
- [32] D.G. Georgiev, P. Boolchand, K.A. Jackson, Intrinsic nanoscale phase separation of bulk As<sub>2</sub>S<sub>3</sub> glass, *Phil. Mag.* 83 (2003) 2941.
- [33] J.D. Musgraves, P. Wachtel, B. Gleason, K. Richardson, Raman spectroscopic analysis of the Ge-As-S chalcogenide glass-forming system, *J. Non-Crystalline Solids* 386 (2014) 61–66.
- [34] Roberto Forneris, The infrared and raman spectra of realgar and orpiment, *The American mineralogist*, vol. 54, July-August, 1969, 1062–1074.
- [35] W.L. Konijnendijk, J.M. Stevels, The structure of borosilicate glasses studied by Raman scattering, *J. Non-Crystalline Solids* 20 (2) (1976) 193–224.
- [36] L. De Ferri, P.P. Lottici, G. Vezzalini, Characterization of alteration phases on Potash–Lime–Silica glass, *Corrosion Sci.* 80 (2014) 434–441.
- [37] Q. Mei, R.T. Hart, C.J. Benmore, S. Amin, K. Leinenweber, J.L. Yarger, The structure of densified As<sub>2</sub>O<sub>3</sub> glasses, *J. Non-Crystalline Solids* 353 (18–21) (2007) 1755–1758.
- [38] L. Sirloto, A. Vergara, M.A. Ferrara, Advances in stimulated Raman scattering in nanostructures, *Adv. Optics Photonics* 9 (1) (2017) 169.